Electronic Supplementary Material (ESI) for Journal of Materials Chemistry

Electronic supplementary information for

Dramatic enhancements in toughness of polyimide nanocomposite via long-CNT-induced long-range creep†

Xilai Jia,[a] Qiang Zhang,[a,] Meng-Qiang Zhao,[a] Guang-Hui Xu,[a] Jia-Qi Huang,[a] Weizhong Qian,[a] Yunfeng Lu,[b,*] and Fei Wei[a,c,*]*

[a] Beijing Key Laboratory of Green Chemical Reaction Engineering and Technology, Department of Chemical Engineering, Tsinghua University, Beijing 100084, P.R. China

[b] Departments of Chemical Engineering and Materials Science Engineering, University of California, Los Angeles, California 90095, USA

[c] Center for Nano and Micro Mechanics, Tsinghua University, Beijing 100084, P. R. China

E-mails: zhang-qiang@mails.tsinghua.edu.cn; luucla@ucla.edu; wf-dce@tsinghua.edu.cn;

Fax: +86-10-6277-2051; Tel: +86-10-6278-5464

Table S1. Summary of mechanical properties of the neat PI and tough 0.27 wt% CNT/PI composite compared with conventional tough materials.

Materials	tensile strength (MPa)	Failure strain (%)	Young's modulus (GPa)	Toughness (kJ/kg)
PI	81.9	42	0.96	22.4
CNT/PI	152	150	1.013	127.4
Steel	800	1.5		12
Kevlar	4000	5	130	33
Nylon	60			60
Rubber	1	600	-	80
Spider silk	1300-2000	20-40	30	100-400

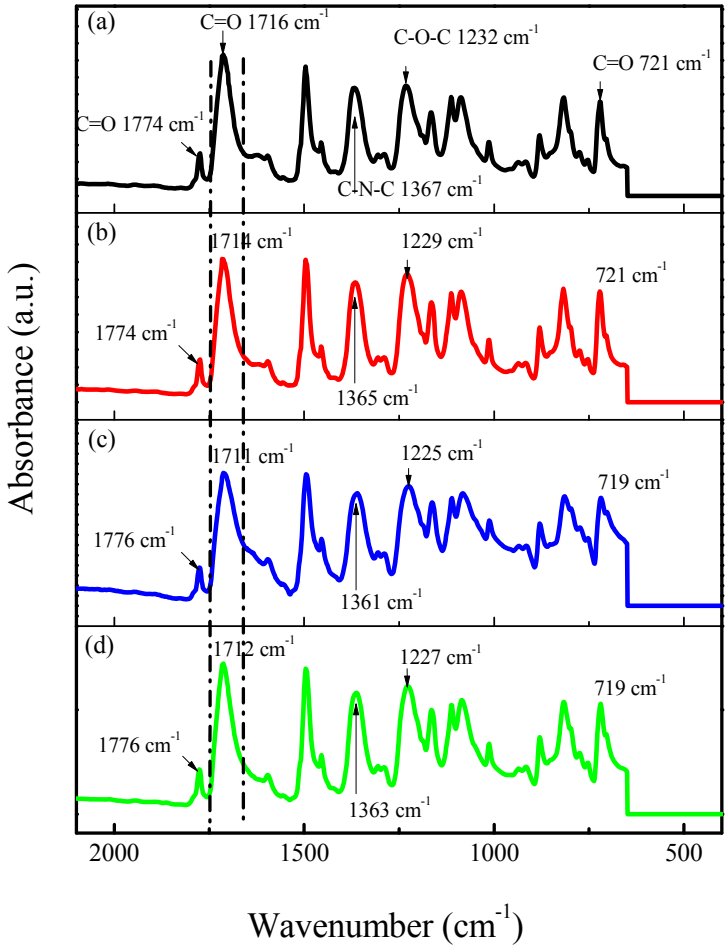

Fig. S1. ATR-FTIR spectra of the as-fabricated nanocomposite films: (a) neat PI, (b) CNT/PI, (c) w-CNT/PI, and (d) s-CNT/PI. Chemical structures of neat PI and the nanocomposite films were detected by ATR-FTIR spectra shown in Fig. S1. For neat PI (Fig. S1a), the characteristic absorption bands of the amide carbonyl stretching were observed at 1774 and 1716 cm^{-1}. The C-N stretching for the imide linkage was at 1367 cm^{-1} and the C=O bending peak was at 721 cm^{-1}. When the 0.27 wt% purified CNTs were added, no new absorbance bands appeared (Fig. S1b). The interaction between CNTs and matrix was the non-covalent wrapping of PI backbone by π-π stacking on the CNT sidewall. When the weakly and strongly oxidized CNTs were added into the matrix, the carboxylic acid groups react with the amine groups from PI precursor. The blue shift of C=O stretching from 1716 to 1712 cm^{-1} suggested that the amide carbonyl had been affected by oxidized nanotube addition (Fig. S1c and Fig. S1d). Moreover, compared to neat PI, the observed peak at 1716 cm^{-1} was broadened, which was ascribed to hydrogen bonding between matrix and carboxylic CNTs.

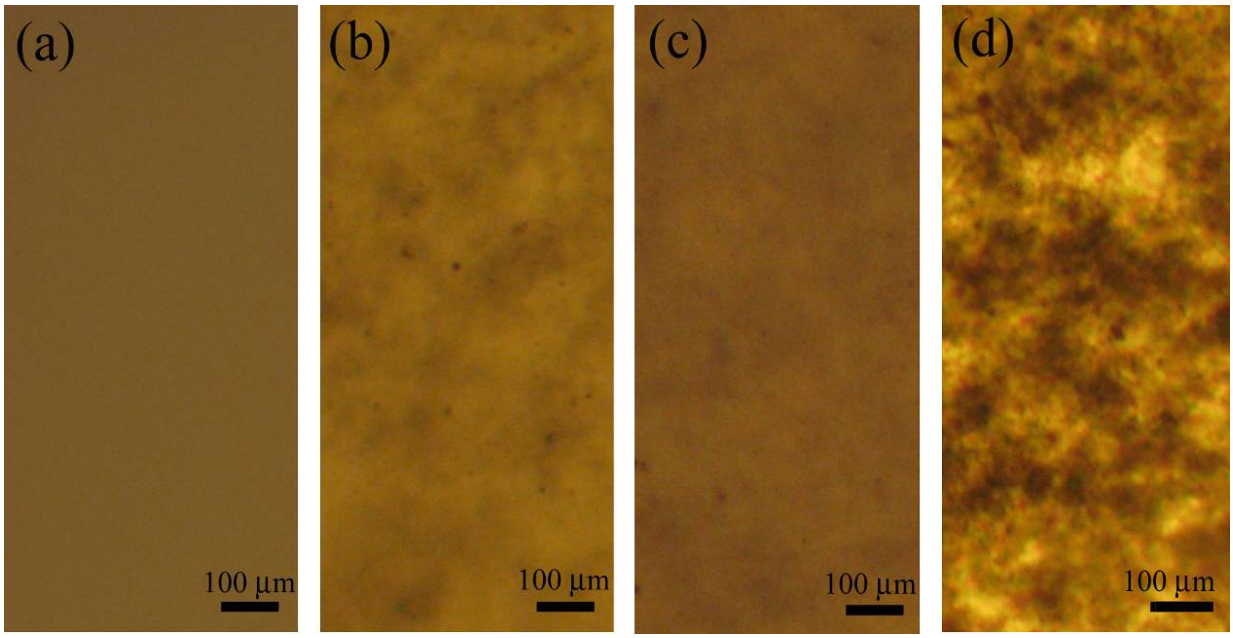

Fig. S2. Optical microscope images of the CNT dispersion states in PI matrix: (a) neat PI, (b) 0.10 wt%, (c) 0.27 wt%, and (d) 0.40 wt% CNT/PI composites. The CNTs showed a good dispersion state in PI matrix at a low nanotube loading (<0.27 wt%) (Fig. S2b, c). With the CNT content increasing to 0.40 wt% (Fig. S2d), CNT aggregates appeared in the composite.

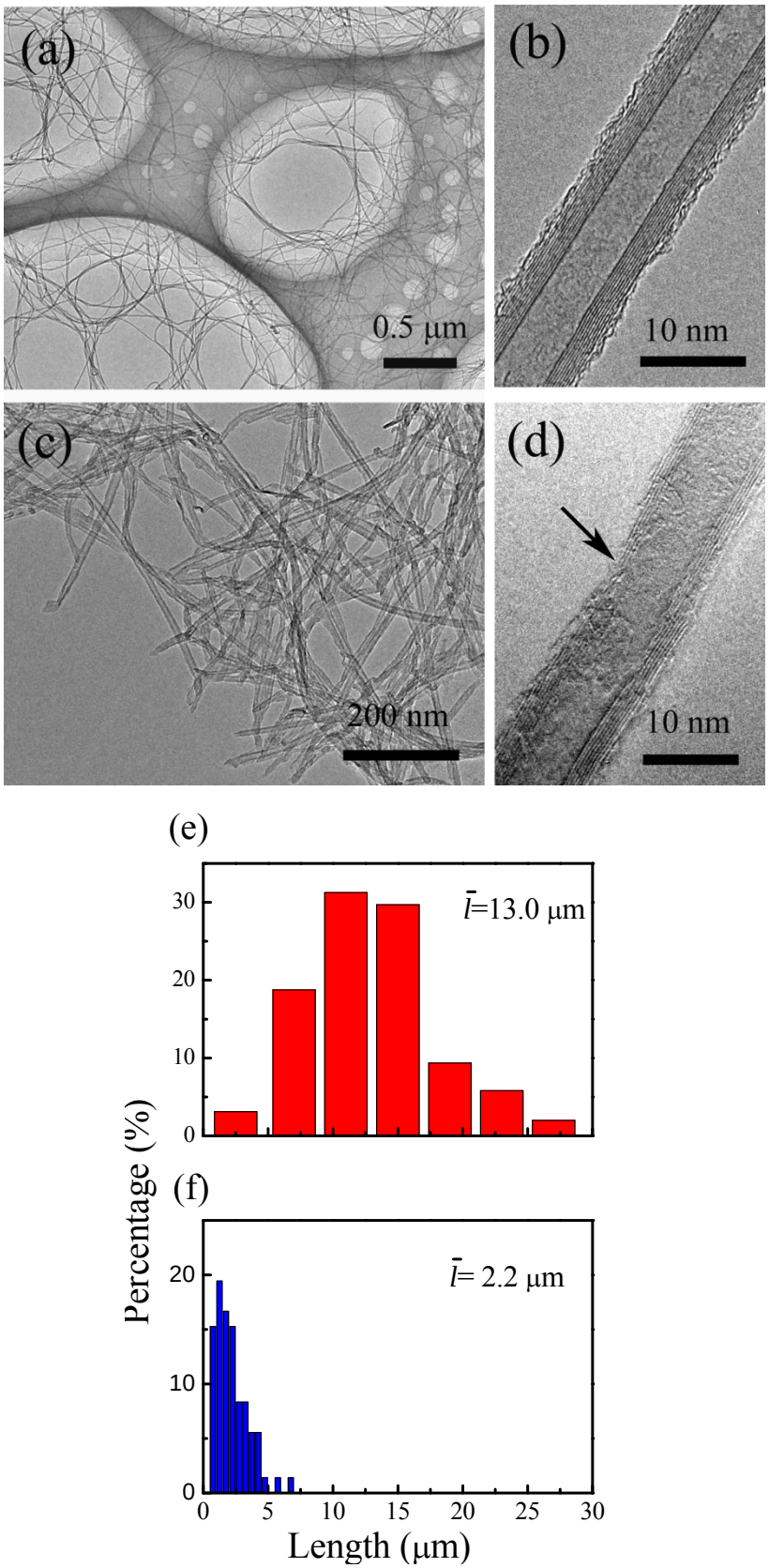

Fig. S3. TEM and HRTEM images of (a,b) the weakly oxidized CNTs (w-CNTs) and (c,d) the strongly oxidized CNTs (s-CNTs). The length distribution of (e) w-CNTs and (f) s-CNTs.

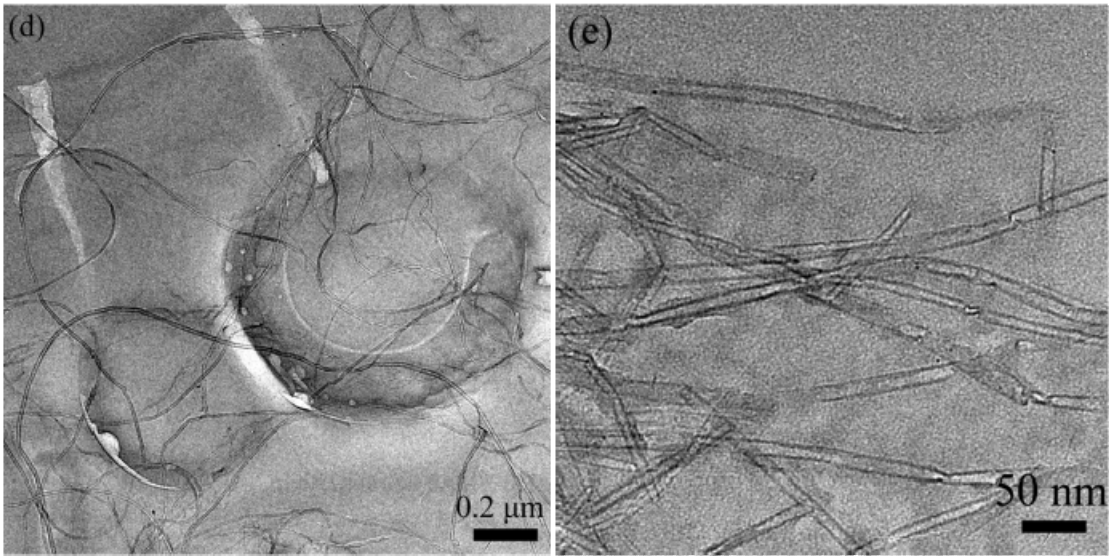

Fig. S4. (a) The weakly oxidized w-CNTs and (b) strongly oxidized s-CNTs in PI matrix.

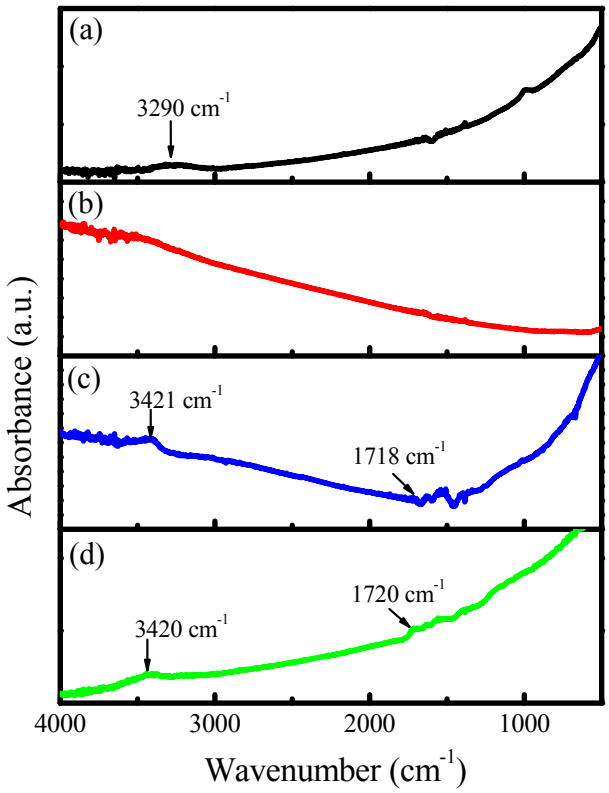

Fig. S5. FTIR spectra of the as-obtained nanotubes: (a) pristine CNTs, (b) purified CNTs, (c) w-CNTs, and (d) s-CNTs. In contrast to the pristine CNT arrays (Fig. S5a), the purified CNTs show almost no obvious absorbance peaks, indicating that such CNTs were not oxidized (Fig. S5b). However, for w-CNTs (Fig. S5c) and s-CNTs (Fig. S5d), new peaks clearly appeared. These peaks were attributed to the generated carboxylic acid groups at the surface of CNTs after the treatment with H_2SO_4/H_2O_2 or H_2SO_4/HNO_3. The absorbance of 1718 (or 1720) cm^{-1} was assigned to C=O stretching and the broad band around 3421 cm^{-1} absorbance was due to –OH groups.

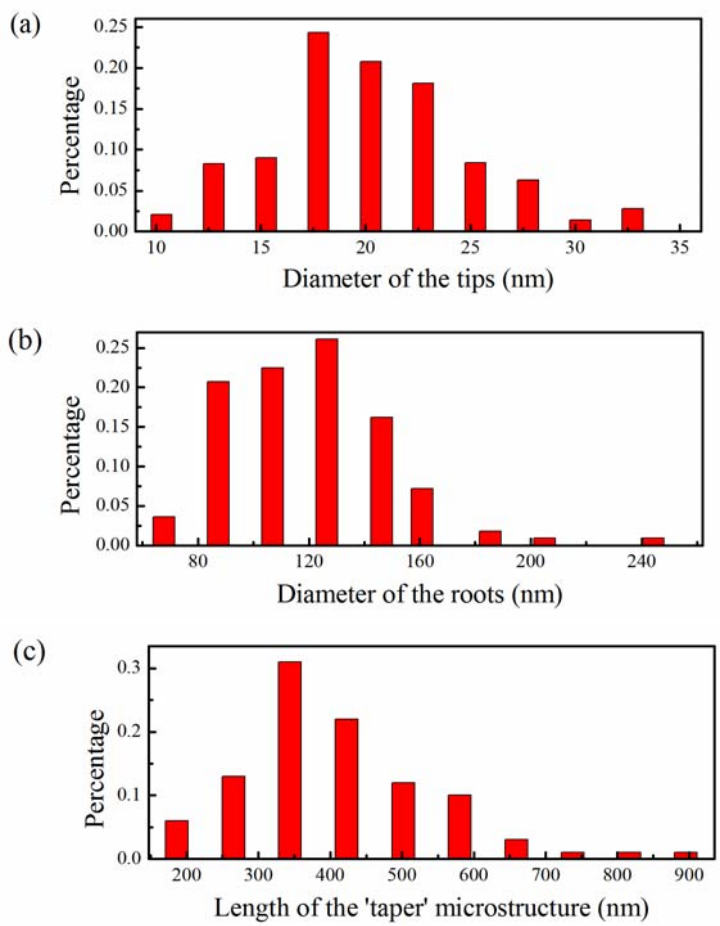

Fig. S6. The size distributions of the taper fibril microstructure on fracture edges: (a) the tip diameter, (b) the root diameter, and (c) the length of the fibrils. The gradient size distributions from fibril tips to roots reveal that PI moves along the sidewall of CNTs after sufficient deformation.

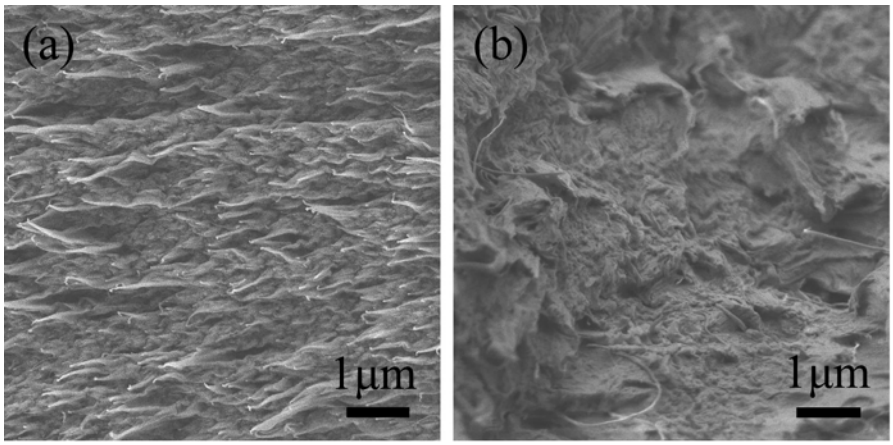

Fig. S7. SEM images of morphology on cross-section of 0.27 wt% (a) w-CNT/PI and (b) s-CNT/PI nanocomposites.

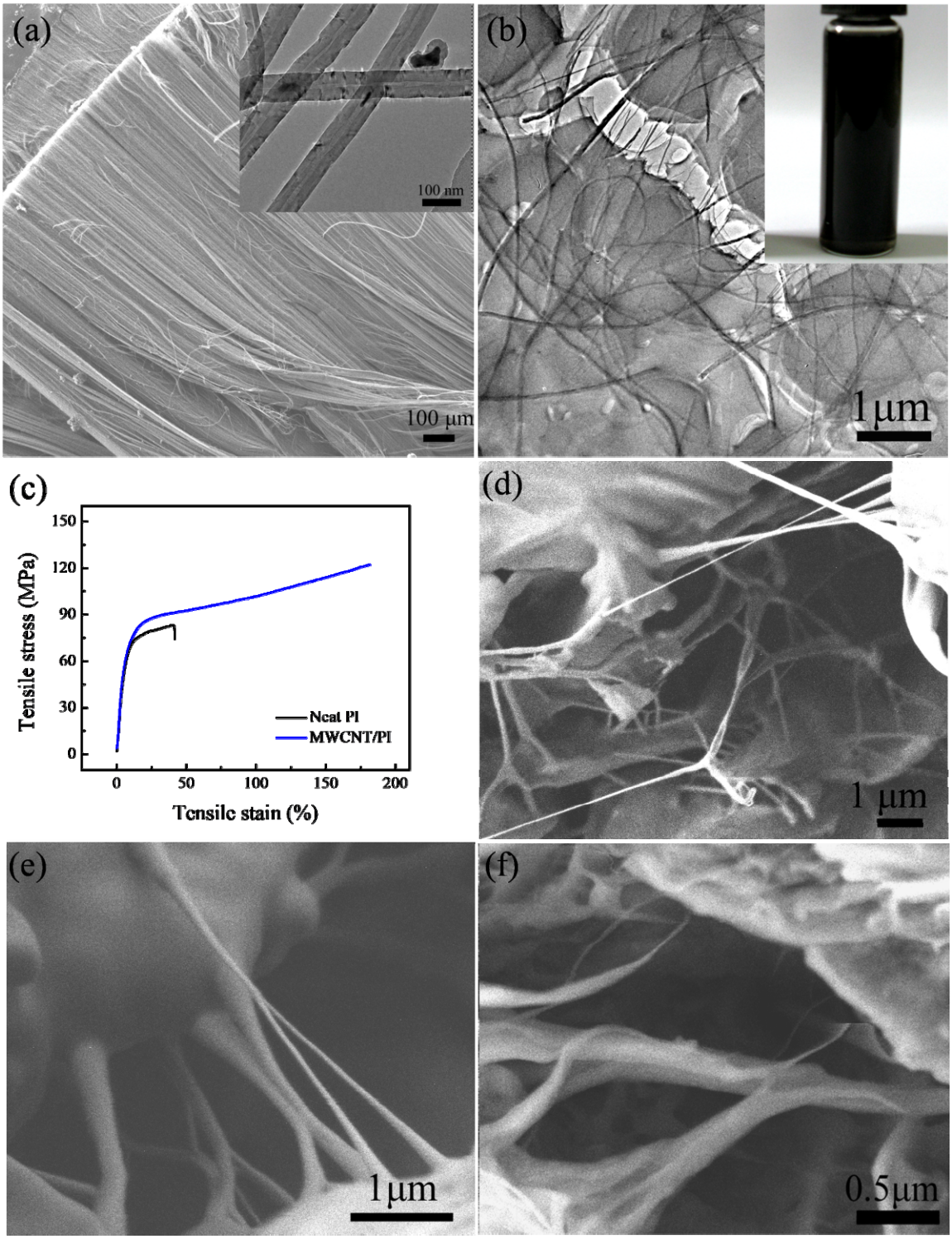

Fig. S8. (a) SEM images of the superlong MWCNTs, inserted figure is the TEM image of such CNTs. (b) TEM image of MWCNT dispersed in a PI matrix (insert is photographs of PAA-CNT-DMAc suspension after 2.0 hr standing). (c) Stress–strain curves of neat PI and 0.30 wt% MCNT/PI nanocomposites. (d-f) SEM images of fracture surfaces of 0.30 wt% MWCNT/PI composites after sufficient deformation: (d) the enlarged CNT network embedded in the matrix; (e) the CNT bridging of cracks and (f) the highly developed taper fibrils.